

Many-body transitions in a single molecule visualized by scanning tunnelling microscopy

Fabian Schulz¹, Mari Ijäs², Robert Drost¹, Sampsa K. Hämäläinen¹, Ari Harju^{2*}, Ari P. Seitsonen^{3,4} and Peter Liljeroth^{1*}

Many-body effects arise from the collective behaviour of large numbers of interacting particles, for example, electrons, and the properties of such a system cannot be understood considering only single or non-interacting particles^{1–5}. Despite the generality of the many-body picture, there are only a few examples of experimentally observing such effects in molecular systems^{6–8}. Measurements of the local density of states of single molecules by scanning tunnelling spectroscopy is usually interpreted in terms of single-particle molecular orbitals^{9–11}. Here, we show that the simple single-particle picture fails qualitatively to account for the resonances in the tunnelling spectra of different charge states of cobalt phthalocyanine molecules. Instead, these resonances can be understood as a series of many-body excitations of the different ground states of the molecule. Our theoretical approach opens an accessible route beyond the single-particle picture in quantifying many-body states in molecules.

Scanning tunnelling microscopy (STM) allows one to investigate the atomic-scale structure and electronic properties of surfaces and adsorbates. It probes the local density of states (LDOS), enabling direct visualization of the energy and symmetry of molecular electronic orbitals. If an ultrathin insulating layer electronically decouples the molecules from the substrate^{9,12}, their resonances can be measured with great detail by scanning tunnelling spectroscopy (STS), allowing the identification of, for example, vibronic satellites^{8,12–14}. Although there are several examples of many-body (MB) phenomena investigated by STM in solid-state systems^{15–20}, such effects are usually neglected when interpreting images and tunnelling spectra of single molecules^{9–11}. A prominent exception is the Kondo effect, a MB singlet ground state formed between an unpaired spin in a molecule and a screening cloud of quasi-free electrons^{6,7}. However, the Kondo effect arises owing to the interaction with the electron Fermi sea of the substrate and, thus, is not an intrinsic MB state of the molecule. Quantum chemistry calculations predict the mixing and distortion of molecular single-particle (SP) wavefunctions due to electron correlation^{21,22}, which would be an intrinsic MB effect. Nevertheless, most of the predicted effects are subtle and, so far, there is no clear experimental verification of MB transitions in single molecules. Probing excited states in single molecules by tunnelling spectroscopy, we demonstrate the existence of MB effects arising purely from electronic states confined in the molecule.

We have carried out low-temperature STM experiments on cobalt phthalocyanine molecules (CoPC) adsorbed on monolayer hexagonal boron nitride (h-BN) grown on an Ir(111) substrate.

Owing to the large work function modulation over the h-BN/Ir(111) moiré unit cell, we can carry out differential conductance (dI/dV) spectroscopy on CoPC molecules that are initially in different charge states^{14,23}. The observed resonances in the dI/dV spectra cannot be explained within the single-electron picture. Instead, we have to consider the many-body spectral function, estimated based on time-dependent density functional theory (TDDFT) calculations. This computationally accessible approach is sufficient to obtain both the energies and spatial dependence of the molecular resonances with high accuracy.

Figure 1a is a schematic representation of our sample system: a monolayer of h-BN is grown on the surface of an Ir(111) single crystal (see Methods for details)^{23,24}. The lattice mismatch between h-BN and the Ir(111) surface results in a moiré superstructure, comprised of regions with strong ('pores') and weak ('wires') h-BN/metal interaction. Topography, work function and chemical reactivity of the h-BN layer are modulated along the moiré pattern²³, which acts as a nanotemplate and results in preferred CoPC adsorption on the pores¹⁴. Once the pores are occupied, the molecules also adsorb on the wire regions. CoPC remains in a neutral charge state (CoPC⁰) on the wire and becomes negatively charged (CoPC⁻¹) on the pores¹⁴, which is reflected by the different molecular contrasts in the STM topography in Fig. 1b.

Electronic states of the molecule result in peaks in the dI/dV signal of the STM junction^{9,12}. Typical spectra for neutral and anionic CoPC are shown in Fig. 1c and d, respectively. CoPC⁰ exhibits three characteristic resonances: in the unoccupied LDOS at positive bias, we find one resonance at ~ 0.9 V (labelled N2) localized at the metal centre and one at ~ 1.7 V (N1) delocalized over the carbon backbone, which we assign within the SP picture to the LUMO and LUMO+1, respectively. Another delocalized resonance exists in the occupied part at ~ -1.0 V (N3), and consequently is assigned to the HOMO. In addition, all three resonances show satellite peaks due to the inelastic excitation of vibrations in the molecule^{8,12,25,26}. The spacing of the vibronic replica (labelled N1v, N2v, N3v and so on) indicates a dominant vibrational mode with an energy of ~ 100 meV (ref. 14). For the remainder of the paper, we reference all the orbitals with respect to their order in neutral CoPC.

The dI/dV spectra of CoPC⁻¹ exhibit only one delocalized peak (labelled A1) in the unoccupied part at ~ 0.7 V, which should thus correspond to the LUMO+1 of the neutral molecule. The first peak at negative bias is at ~ -0.1 V (A2) and marks the—now occupied—LUMO. Both the LUMO and LUMO+1 have shifted down in energy by roughly 1 eV on charging. In the SP picture, the charging of the molecule would lead simply to a downward shift of

¹Department of Applied Physics, Aalto University School of Science, PO Box 15100, 00076 Aalto, Finland. ²COMP Centre of Excellence, Department of Applied Physics, Aalto University School of Science, PO Box 11100, 00076 Aalto, Finland. ³Institut für Chemie, University of Zürich, Winterthurerstrasse 190, CH-8057 Zürich, Switzerland. ⁴École Normale Supérieure, Département de Chimie, 24 rue Lhomond, F-75005 Paris, France.

*e-mail: ari.harju@aalto.fi; peter.liljeroth@aalto.fi

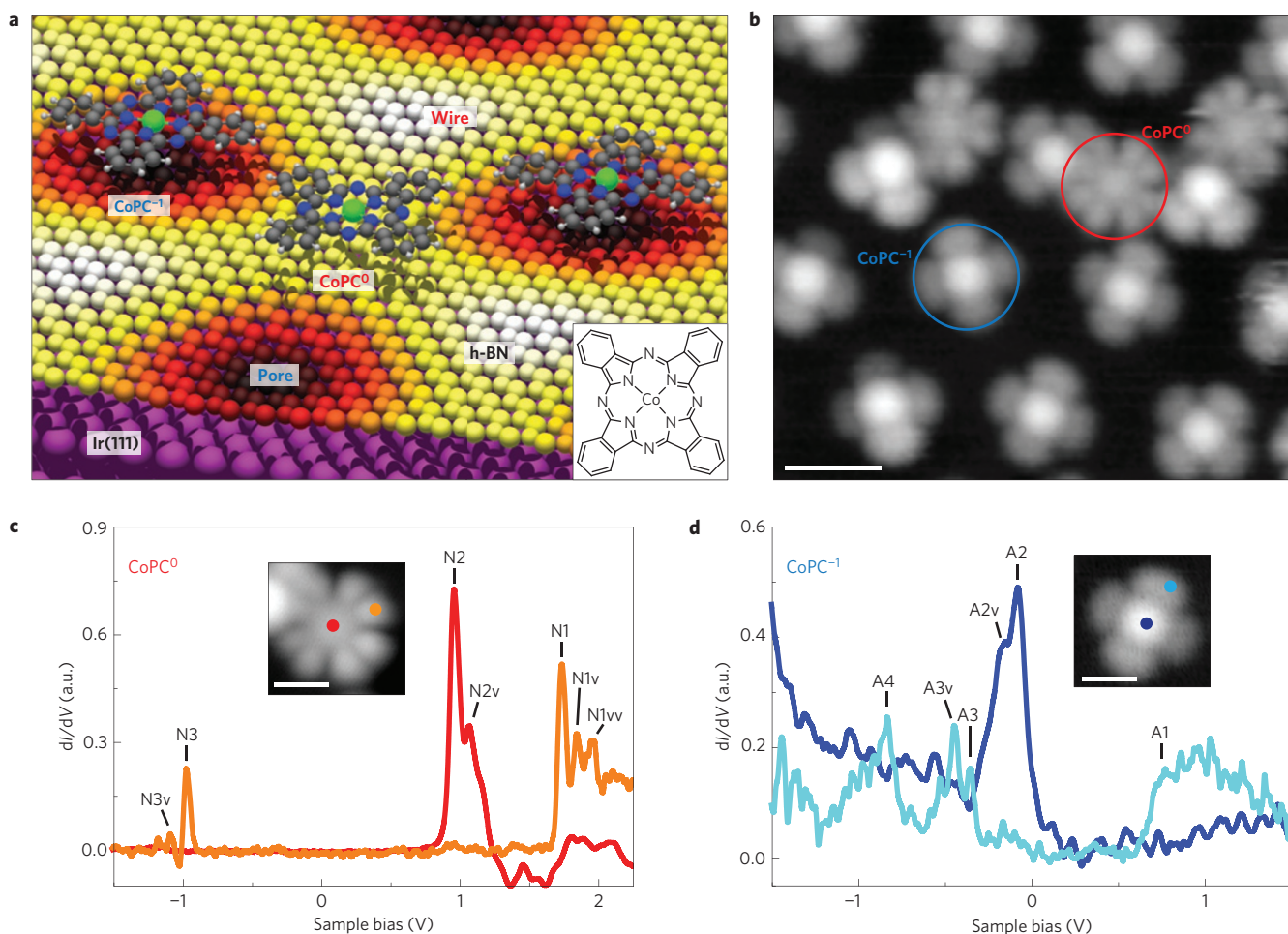


Figure 1 | Schematic of the experiment and spectroscopy on the two charge states of CoPC on h-BN on Ir(111). **a,b**, Schematic picture (**a**) and an STM image (**b**) of CoPC molecules adsorbed on a h-BN monolayer on Ir(111). Inset in **a** shows the chemical structure of CoPC. Scale bar in **b** is 2 nm; tunnelling parameters are -2.05 V, 4 pA. **c,d**, dI/dV spectra acquired on a neutral (**c**) and negatively charged (**d**) CoPC molecule adsorbed on the wire and pore regions of the moiré unit cell, respectively. The resonances and their vibronic replica are labelled with N and A, referring to resonances of the neutral and anionic species, respectively. Insets show STM images indicating the position of the spectra. Scale bars are 1 nm, tunnelling parameters are -2.00 V, 3 pA (**c**) and -2.05 V, 5 pA (**d**).

all orbitals. Therefore, the next-lowest transition, corresponding to the HOMO of neutral CoPC, should appear around -2 V; that is, no further resonance should be detected within the energy range of the spectrum in Fig. 1d. Instead, we find two further resonances in close proximity to the LUMO, at ~ -0.3 V (A3) and ~ -0.8 V (A4). Even though the exact energies of the resonances can vary by a few hundreds of meV between different molecules owing to slight changes in the adsorption position, the overall sequence of the observed peaks is always the same and the relative energy differences do not vary significantly. Our experiments suggest a profound modification of the electronic transitions of the molecule, inconsistent with the SP picture. The molecule is decoupled from the substrate by the ultrathin insulating h-BN layer¹⁴, which has negligible DOS around the Fermi level²³. Therefore, these deviations represent the intrinsic electronic properties of the molecule.

In STS, we either inject an electron into the molecule on the unoccupied part of the LDOS or remove an electron from the occupied part. Thus, we measure transitions from an N -electron initial state into $(N \pm 1)$ -electron final states. Because the experiments are performed at low temperature, the initial state is always assumed to be the ground state, whereas the final states can also correspond to excited states. In the usual SP picture, the final states would be directly obtained by occupying or unoccupying the orbitals of the molecule's ground state in their respective order. This

is illustrated in Fig. 2 (bottom row) for electron removal from a charged molecule (spectra at negative bias on the pore molecules) and for electron addition into a neutral molecule (spectra at positive bias on the wire molecules).

However, two important effects are neglected when treating electronic transitions in the SP picture: reordering of molecular orbitals due to the interaction of the additional electron or hole with the other electrons, and contributions of multiple SP excitations to the excited states due to correlation effects. In the MB picture, the STS response is given by the diagonal elements of the MB spectral function, for example, for a transition from an N - into an $(N + 1)$ -electron state

$$A(\nu, E) = 2\pi \sum_k \left| \langle \Psi_k^{N+1} | c_\nu^\dagger | \Psi_0^N \rangle \right|^2 \delta(E - E_k^{N+1} + E_0^N)$$

Here, the index ν refers to the orbitals of the SP basis and E_k^N to the energy of the different MB states. $k = 0$ denotes the ground state of the molecule, whereas the excited states are denoted by $k = 1, 2, 3, \dots$. The transition is described as occupying the orbital ν by applying the creation operator c_ν^\dagger to the initial state $|\Psi_0^N\rangle$ to reach the final state $|\Psi_k^{N+1}\rangle$. The δ -function assures that only transitions satisfying energy conservation are considered. Writing the energy of the excited states as $E_k^{N+1} = E_0^{N+1} + \Delta E_k^{N+1}$, it is seen that the peaks

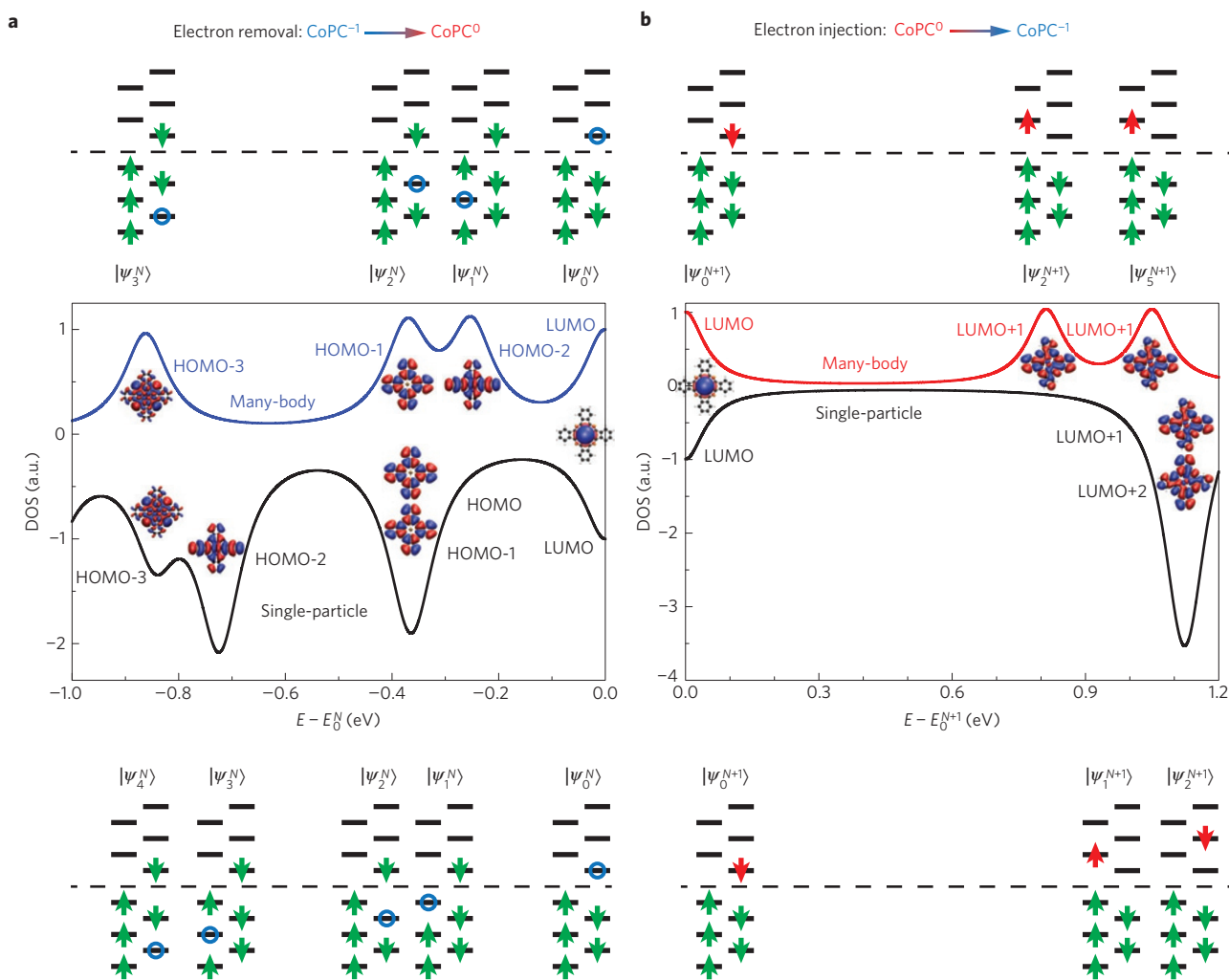


Figure 2 | Comparison between transitions in the single-particle and many-body pictures. **a, b**, Schematic representations of the calculated transitions for electron removal from the CoPC^{-1} (**a**) and electron addition to the CoPC^0 ground state (**b**). The bottom and top rows depict the expected transitions within the single-particle (SP) and many-body (MB) pictures, respectively. In case of the MB excited states, only the dominant contributions on projection onto the SP wavefunction basis set are shown. Arrows and circles represent electrons and holes, respectively. The dashed line indicates filling up to charge neutrality. The middle panels show simulated DOS based on the SP ('negative' DOS) and MB ('positive' DOS) transitions. The transition into the ground state, that is, the LUMO, is set to zero energy. The transitions in the upper and bottom row are aligned with the corresponding peaks in the DOS.

in the STS spectra are separated by the energy differences between the excited and ground states.

We account for the two effects described above by first calculating the ground states of the different charge states separately by standard DFT and subsequently approximating the MB excited states with TDDFT. The DFT calculation of the different charge states already includes some MB effects (in the exchange–correlation functional). Although ground-state DFT predicts a reordering of the orbitals on charging (see Supplementary Information for details), this effect is further modified in TDDFT. Moreover, contributions from multiple SP excitations to the excited states are not contained within standard DFT. We decompose the excited states computed with TDDFT onto a basis set of SP wavefunctions, in our case the molecular orbitals of neutral CoPC . This allows us to directly compare the MB excited states with those expected from the SP picture in a computationally accessible way.

The results of the TDDFT calculations are summarized in Fig. 2 (top row). The schematic shows only MB excited states which can be obtained by a single tunnelling event and, of those transitions, only the dominant contribution on projection onto the SP wavefunctions is indicated (Supplementary Information). We find significant

deviations of the spectral functions from the SP picture due to MB effects. When removing an electron from CoPC^{-1} , the first and third excited state, $|\Psi_1^N\rangle$ and $|\Psi_3^N\rangle$, correspond to emptying the HOMO-2 and HOMO-3 instead of the HOMO and HOMO-2, respectively. For the injection of an electron into CoPC^0 , both the second and fifth excited state, $|\Psi_2^{N+1}\rangle$ and $|\Psi_5^{N+1}\rangle$, correspond to the occupation of the LUMO+1.

Even though the decomposition of the MB excited states into SP excitations indicates only weak orbital mixing (Supplementary Information), this is sufficient to lift the degeneracy of $|\Psi_2^{N+1}\rangle$ and $|\Psi_5^{N+1}\rangle$. This can be seen in the middle panels of Fig. 2a and b, which compare the predicted DOS in the SP and MB pictures. The change in orbital order and their mixing significantly changes the energies at which the excited states are observed. In particular, both the first and second MB excited states for electron removal from CoPC^{-1} are closer in energy to the ground state than the first SP excited state, thus offering a potential explanation for the features observed in our tunnelling spectra.

Further proof for the experimental identification of these MB transitions comes from their predicted spatial dependence. Their intensities are directly related to the square of the wavefunction

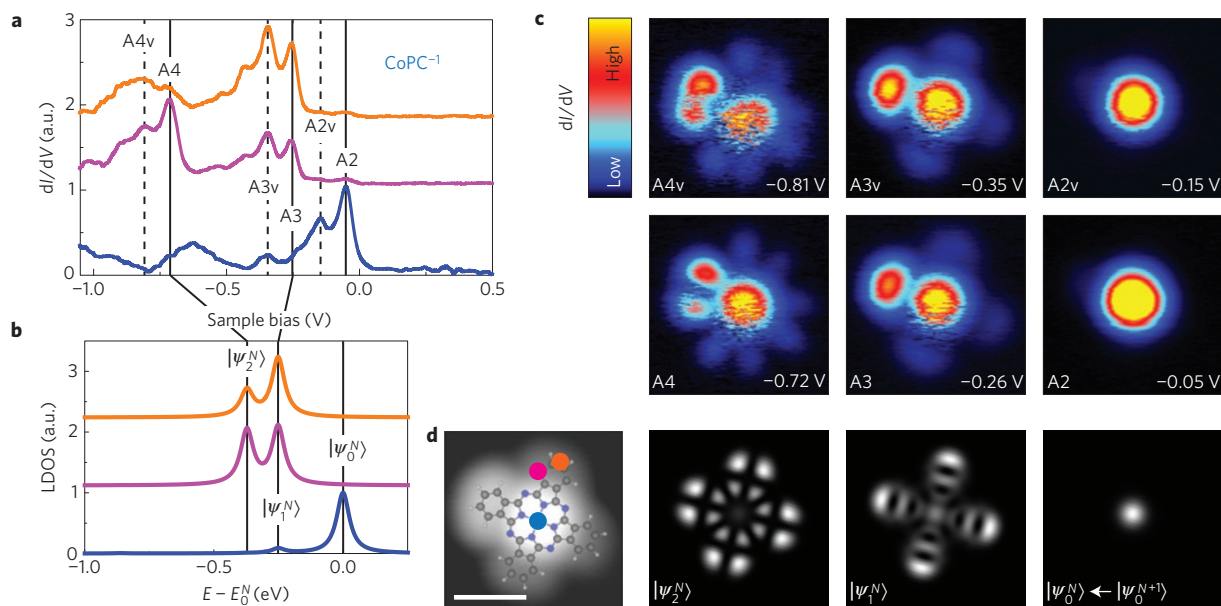


Figure 3 | Wavefunction mapping on the negatively charged CoPC. **a, b**, Experimental high-resolution dI/dV spectra (**a**) and simulated LDOS (**b**) on different points over the CoPC^{-1} . Spectra are offset for clarity. The hump at ~ -0.65 V in the blue spectrum in **a** was not reproducibly found on other molecules (see Supplementary Information) and thus not assigned to a molecular resonance. **c**, Experimental dI/dV maps at different energies, corresponding to the different resonances (middle row) and their vibronic replica (upper row). The lower row shows simulated LDOS maps for the MB transitions from CoPC^{-1} to CoPC^0 . **d**, STM image overlaid with the structural model of CoPC, indicating the positions of the experimental and simulated spectra, respectively. Scale bar is 1 nm, tunnelling parameters are -1.51 V, 8 pA.

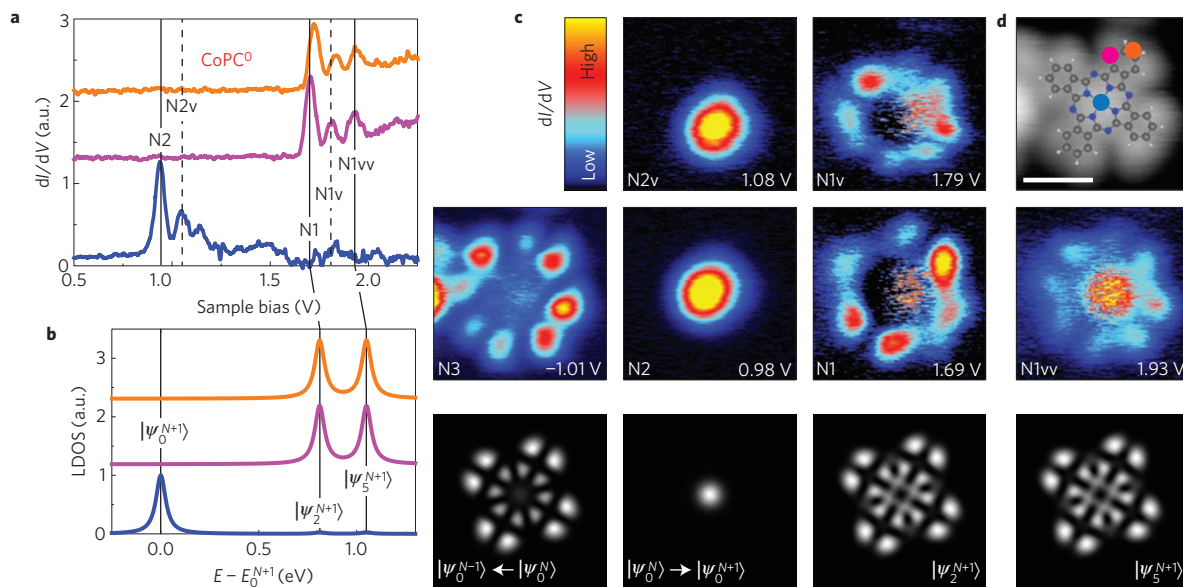


Figure 4 | Wavefunction mapping on the neutral CoPC. **a, b**, Experimental high-resolution dI/dV spectra (**a**) and simulated LDOS (**b**) on different points over the CoPC^0 . Spectra are offset for clarity. **c**, Experimental dI/dV maps at different energies, corresponding to the different resonances (middle row) and their vibronic replica (upper row). The lower row shows simulated LDOS maps for the MB transitions from CoPC^0 to CoPC^{-1} , as well as from CoPC^0 into the CoPC^{+1} ground state at negative energy. **d**, STM image overlaid with the structural model of CoPC, indicating the positions of the experimental and simulated spectra, respectively. Scale bar is 1 nm, tunnelling parameters are -2.00 V, 2 pA.

of the states from which or into which the tunnelling occurs. The dI/dV spectra taken on different positions over the CoPC molecule can be simulated by multiplying the total DOS shown in Fig. 2 by the squares of the relevant wavefunctions at the position of the STM tip. Figure 3a shows experimental high-resolution spectra taken on three different positions over CoPC^{-1} . Clearly, the relative intensities of the A2, A3 and A4 resonances change with position. This is in good agreement with the simulated spectra for

the ground state $|\Psi_0^N\rangle$ and the MB excited states $|\Psi_1^N\rangle$ and $|\Psi_2^N\rangle$ (Fig. 3b), and directly reflects the different symmetries and nodes of the wavefunctions involved in the transitions (see Supplementary Information for simulated SP spectra). Their shape and symmetry can be directly visualized by recording the dI/dV signal in the constant-height mode, allowing comparison with simulated LDOS maps (Fig. 3c). The wavefunctions of the excited states $|\Psi_1^N\rangle$ and $|\Psi_2^N\rangle$ both have four-fold symmetry but different nodal planes.

Comparing our experimental dI/dV maps with the simulation, we can unambiguously match resonances A3 and A4 and their vibronic replica to the MB excited states $|\Psi_1^N\rangle$ and $|\Psi_2^N\rangle$, respectively. The slight asymmetry in the experimental dI/dV maps is due to a tilting of the molecule (see topography in Fig. 3d and Supplementary Information for additional data and for discussion of the increased intensity in the centre of CoPC).

We can carry out a similar analysis for the neutral CoPC⁰ (Fig. 4). This shows that the intensity and position of peak N1v is inconsistent with assigning it to a second vibronic satellite of resonance N1. Intensities of vibronic replicas should follow a Poisson distribution^{25,26}; hence, N1vv also should have much lower intensity than the first vibronic replica N1v. The extra intensity in our spectra cannot originate from an additional high-energy vibrational mode (Fig. 4a), as the spacing between the elastic peaks N1 and N1vv is around 0.22 V, which does not fit the known vibrational modes for CoPC (ref. 27). However, this resonance can be easily interpreted within the MB picture. The resonance N1 corresponds to the MB excited state $|\Psi_2^{N+1}\rangle$. The next MB transition observable in STM is $|\Psi_5^{N+1}\rangle$, predicted to appear only 0.24 eV above $|\Psi_2^{N+1}\rangle$ and corresponding to tunnelling into the same orbital (Fig. 4b). Therefore, we assign peak N1vv to tunnelling into the many-body excited state $|\Psi_5^{N+1}\rangle$ instead of originating from electron–vibration coupling (see Supplementary Information for discussion of the small discrepancy between simulated LDOS and experimental maps^{8,13}).

The summary of the comparison between the overall predictions of the SP picture, standard DFT in the different charge states (that can include, for example, orbital reordering effects) and the MB picture based on TDDFT calculations can be found in the Supplementary Information. The MB calculations based on TDDFT provide the highest overall agreement with the experiment for both charge states. Standard DFT of the negatively charged CoPC also captures partially the reordering of the orbitals (which is a many-body effect). The MB calculation captures all the resonances correctly, including the significant splitting of the higher orbitals at positive bias, and the reordering of the orbitals at the negative bias. On the other hand, the splitting of the higher resonances at negative bias is underestimated by the MB treatment based on TDDFT.

Finally, the resonance N3, for which the map is shown in Fig. 4c, should correspond to the transition from the N -electron ground state into the $(N - 1)$ -electron ground state—that is, an electron tunnelling out of the HOMO. Here, no deviation of the many-body picture from the single-particle picture is expected. Indeed, the experimentally measured dI/dV map resembles the shape and symmetry of the calculated HOMO wavefunction. This observation further proves the reordering of the molecular orbitals due to MB effects, as the experimentally measured LDOS for the first transition (N3, A3) below the LUMO (N2, A2) clearly yields different wavefunctions for the neutral and negatively charged CoPC.

Methods

Sample preparation. All sample preparations and experiments were carried out in an ultrahigh vacuum system with a base pressure of $\sim 10^{-10}$ mbar. The (111)-terminated iridium single crystal was cleaned by repeated cycles of Ne⁺ sputtering at 1.5 kV, annealing to 900 °C in a 5×10^{-7} mbar oxygen atmosphere and subsequent flashing to 1,400 °C. Monolayers of h-BN were grown by chemical vapour deposition of borazine (B₃N₃H₆), with the sample held at a temperature of 1,080 °C and a borazine pressure of 2×10^{-8} mbar (ref. 23). CoPC molecules were evaporated from a Knudsen cell at 375 °C onto the h-BN/Ir(111) substrate at room temperature.

STM measurements. After the preparation, the sample was inserted into the low-temperature STM and all subsequent experiments were performed at 5 K. STM images were taken in the constant current mode. dI/dV spectra were recorded by standard lock-in detection while sweeping the sample bias in an open feedback loop configuration, with a peak-to-peak modulation of the sample

bias of 20 mV at a frequency of 526 Hz. Typical parameters for opening the feedback loop were tunnelling currents of 20–50 pA at -2 V sample bias. dI/dV maps were recorded in the constant-height mode and at peak-to-peak modulations of 20–30 mV. A typical procedure to record a constant-height dI/dV map started by positioning the tip over the h-BN layer at feedback parameters of 6 pA at -2 V, then opening the feedback loop, setting the sample bias to the desired value and retracting the tip by 1 Å, and finally taking an image with simultaneously recording of the dI/dV signal from the lock-in.

DFT calculations. The orbital wavefunctions for isolated molecules in the absence of a substrate required for the STM and STS simulations were calculated within the DFT formalism as implemented in the all-electron FHI-aims code²⁸, developed at the Fritz-Haber Institute. The tight basis defaults with the cutoff distance of the Co atoms increased to 6 Å and the PBE (ref. 29) functional were used in the calculations. The atomic ZORA approximation was used to describe relativistic effects of the central Co atoms. The structures for the two different charge states were relaxed until the forces acting on atoms were less than 0.001 eV Å⁻¹ and the self-consistent cycle was converged to $\Delta E < 10^{-6}$ eV. The LDOS maps and STS spectra were calculated as in ref. 30, broadening the resonances in the energy space by $\eta = 30$ meV and mapping the wavefunctions 3.5 Å above the molecular plane. The finite size of the STM tip was taken into account in the simulation of the STS spectra by including a spherical region around the measurement point, weighted by a Gaussian of the form $e^{-(r-r_0)^2/\sigma}$, with $\sigma \approx 2.6$ Å. The results were not sensitive to the precise value of σ .

TDDFT calculations. The TDDFT calculations were performed using the code TurboMole (<http://www.turbomole.com>). PBE (ref. 29) was again employed as the exchange–correlation functional, together with the DFT-D3 correction scheme³¹ for the London dispersion forces between the ionic cores missing in PBE. The wavefunctions were expanded with the triple-zeta valence doubly polarized (TZVPP) basis set on all atoms. Strict convergence criteria were required for self-consistency. The excitation energies were calculated using the linear response approach, and the decomposition to the SP orbitals was evaluated using the coefficients of the linear response vectors.

Received 3 July 2014; accepted 26 November 2014;
published online 19 January 2015

References

- Cronenwett, S. M., Oosterkamp, T. H. & Kouwenhoven, L. P. A tunable Kondo effect in quantum dots. *Science* **281**, 540–544 (1998).
- Ediger, M. *et al.* Peculiar many-body effects revealed in the spectroscopy of highly charged quantum dots. *Nature Phys.* **3**, 774–779 (2007).
- Hofferberth, S. *et al.* Probing quantum and thermal noise in an interacting many-body system. *Nature Phys.* **4**, 489–495 (2008).
- Kleemann, N. A. J. M. *et al.* Many-body exciton states in self-assembled quantum dots coupled to a Fermi sea. *Nature Phys.* **6**, 534–538 (2010).
- Martin, M. J. *et al.* A quantum many-body spin system in an optical lattice clock. *Science* **341**, 632–636 (2013).
- Zhao, A. *et al.* Controlling the Kondo effect of an adsorbed magnetic ion through its chemical bonding. *Science* **309**, 1542–1544 (2005).
- Fernandez-Torrente, I., Franke, K. J. & Pascual, J. I. Vibrational Kondo effect in pure organic charge-transfer assemblies. *Phys. Rev. Lett.* **101**, 217203 (2008).
- Repp, J., Liljeroth, P. & Meyer, G. Coherent electron–nuclear coupling in oligothiophene molecular wires. *Nature Phys.* **6**, 975–979 (2010).
- Repp, J., Meyer, G., Stojkovic, S. M., Gourdon, A. & Joachim, C. Molecules on insulating films: Scanning-tunneling microscopy imaging of individual molecular orbitals. *Phys. Rev. Lett.* **94**, 026803 (2005).
- Liljeroth, P., Swart, I., Paavilainen, S., Repp, J. & Meyer, G. Single-molecule synthesis and characterization of metal–ligand complexes by low-temperature STM. *Nano Lett.* **10**, 2475–2479 (2010).
- Albrecht, F., Neu, M., Quest, C., Swart, I. & Repp, J. Formation and characterization of a molecule–metal–molecule bridge in real space. *J. Am. Chem. Soc.* **135**, 9200–9203 (2013).
- Qiu, X. H., Nazin, G. V. & Ho, W. Vibronic states in single molecule electron transport. *Phys. Rev. Lett.* **92**, 206102 (2004).
- Pavliček, N., Swart, I., Niedenführ, J., Meyer, G. & Repp, J. Symmetry dependence of vibration-assisted tunneling. *Phys. Rev. Lett.* **110**, 136101 (2013).
- Schulz, F., Drost, R., Hämmäläinen, S. K. & Liljeroth, P. Templated self-assembly and local doping of molecules on epitaxial hexagonal boron nitride. *ACS Nano* **7**, 11121–11128 (2013).
- Wachowiak, A. *et al.* Direct observation of internal spin structure of magnetic vortex cores. *Science* **298**, 577–580 (2002).
- Hanaguri, T. *et al.* A ‘checkerboard’ electronic crystal state in lightly hole-doped Ca_{2-x}Na_xCuO₂Cl₂. *Nature* **430**, 1001–1005 (2004).

17. Gomes, K. K. *et al.* Visualizing pair formation on the atomic scale in the high- T_c superconductor $\text{Bi}_2\text{Sr}_2\text{CaCu}_2\text{O}_{8+\delta}$. *Nature* **447**, 569–572 (2007).
18. Maruccio, G. *et al.* Correlation effects in wave function mapping of molecular beam epitaxy grown quantum dots. *Nano Lett.* **7**, 2701–2706 (2007).
19. Li, G., Luican, A. & Andrei, E. Y. Scanning tunneling spectroscopy of graphene on graphite. *Phys. Rev. Lett.* **102**, 176804 (2009).
20. Grothe, S. *et al.* Quantifying many-body effects by high-resolution Fourier transform scanning tunneling spectroscopy. *Phys. Rev. Lett.* **111**, 246804 (2013).
21. Toroz, D., Rontani, M. & Corni, S. Visualizing electron correlation by means of *ab initio* scanning tunneling spectroscopy images of single molecules. *J. Chem. Phys.* **134**, 024104 (2011).
22. Toroz, D., Rontani, M. & Corni, S. Proposed alteration of images of molecular orbitals obtained using a scanning tunneling microscope as a probe of electron correlation. *Phys. Rev. Lett.* **110**, 018305 (2013).
23. Schulz, F. *et al.* Epitaxial hexagonal boron nitride on Ir(111): A work function template. *Phys. Rev. B* **89**, 235429 (2014).
24. Orlando, F. *et al.* Epitaxial growth of hexagonal boron nitride on Ir(111). *J. Phys. Chem. C* **116**, 157–164 (2012).
25. Wingreen, N. S., Jacobsen, K. W. & Wilkins, J. W. Resonant tunneling with electron–phonon interaction: An exactly solvable model. *Phys. Rev. Lett.* **61**, 1396–1399 (1988).
26. Wingreen, N. S., Jacobsen, K. W. & Wilkins, J. W. Inelastic scattering in resonant tunneling. *Phys. Rev. B* **40**, 11834–11850 (1989).
27. Liu, Z., Zhang, X., Zhang, Y. & Jiang, J. Theoretical investigation of the molecular, electronic structures and vibrational spectra of a series of first transition metal phthalocyanines. *Spectrochim. Acta A* **67**, 1232–1246 (2007).
28. Blum, V. *et al.* *Ab initio* molecular simulations with numeric atom-centered orbitals. *Comput. Phys. Commun.* **180**, 2175–2196 (2009).
29. Perdew, J. P., Burke, K. & Ernzerhof, M. Generalized gradient approximation made simple. *Phys. Rev. Lett.* **77**, 3865–3868 (1996).
30. Ijäs, M. *et al.* Electronic states in finite graphene nanoribbons: Effect of charging and defects. *Phys. Rev. B* **88**, 075429 (2013).
31. Grimme, S., Antony, J., Ehrlich, S. & Krieg, H. A consistent and accurate *ab initio* parametrization of density functional dispersion correction (DFT-D) for the 94 elements H–Pu. *J. Chem. Phys.* **132**, 154104 (2010).

Acknowledgements

This research made use of the Aalto Nanomicroscopy Center (Aalto NMC) facilities and was supported by the European Research Council (ERC-2011-StG No. 278698 PRECISE-NANO), the Academy of Finland through its Centres of Excellence Program (projects no. 250280 and 251748), and the Finnish Academy of Science and Letters. We acknowledge the computational resources provided by the Centro Svizzero di Calcolo Scientifico (CSCS) under the project s425, and by Aalto Science-IT project and Finland's IT Center for Science (CSC).

Author contributions

F.S. performed all the measurements and analysed the experimental data. M.I. and A.P.S. performed the DFT and TDDFT calculations. F.S., P.L. and M.I. wrote the manuscript. P.L. and A.H. conceived and initiated the project. All authors discussed the data and commented on the manuscript.

Additional information

Supplementary information is available in the [online version of the paper](#). Reprints and permissions information is available online at www.nature.com/reprints. Correspondence and requests for materials should be addressed to A.H. or P.L.

Competing financial interests

The authors declare no competing financial interests.